Improving techniques for diagnostics of laser pulses by compact representations

P. SIDORENKO,[1,2,8,*] A. DIKOPOLTSEV,[1,8] T. ZAHAVY,[3,8] O. LAHAV,[1] S. GAZIT,[4] Y. SHECHTMAN,[5] A. SZAMEIT,[6] D. J. TANNOR,[7] Y. C. ELDAR,[3] M. SEGEV,[1] AND O. COHEN[1]

[1]*Department of Physics and Solid State Institute, Technion, Haifa 32000, Israel*
[2]*School of Applied and Engineering Physics, Cornell University, Ithaca, NY York 14853, USA*
[3]*Department of Electrical Engineering, Technion Haifa 32000, Israel*
[4]*Racah Institute of Physics, The Hebrew University, Jerusalem 91904, Israel*
[5]*Biomedical Engineering Department, Technion, 32000 Haifa, Israel*
[6]*Institut für Physik, Universität Rostock, D-18051 Rostock, Germany*
[7]*Department of Chemical and Biological Physics, Weizmann Institute of Science, Rehovot 76100, Israel*
[8]*These authors contributed equally to this work*
[*]*sidpav@gmail.com*

Abstract: We propose and demonstrate, numerically and experimentally, use of sparsity as prior information for extending the capabilities and performance of techniques and devices for laser pulse diagnostics. We apply the concept of sparsity in three different applications. First, we improve a photodiode-oscilloscope system's resolution for measuring the intensity structure of laser pulses. Second, we demonstrate the intensity profile reconstruction of ultrashort laser pulses from intensity autocorrelation measurements. Finally, we use a sparse representation of pulses (amplitudes and phases) to retrieve measured pulses from incomplete spectrograms of cross-correlation frequency-resolved optical gating traces.

1. Introduction

During the past decade, it has been demonstrated that using sparsity as prior knowledge (henceforth "prior") can be very powerful in extending and improving the performance of many optical measurement devices [1–9]. Essentially, sparsity refers to the fact that the sought information can be expressed in a compact form in some mathematical representation or dictionary [10]. The dictionary is typically assumed to be known in advance, but more generally, can be learned from the measurements under certain conditions [11] or from data with similar features that are often available from other sources [12]. In this sense, sparsity corresponds to the fact that the sought signal has some characteristic structure. Sparsity has been applied in many applications in optics, including single-pixel camera [4], super-resolution [1–3], compressive holography [5], compressive ghost imaging [6], diagnostics of coherent modes [7], un-mixing of spectral measurements [8], and Ankylography for recovering 3D structures of complex molecules [9]. A field in which the sparsity prior has not been extensively utilized yet is diagnostics of ultrashort laser pulses.

Multiple techniques were developed over the years for diagnostics of short and ultrashort laser pulses. In direct measurement techniques, e.g., photodiode-oscilloscope systems that are used for measuring nanosecond to picosecond pulses [13] and streak cameras that can measure pulses with down to 100fs pulse duration [14], only the intensity profile of the pulse can be measured. Intensity Auto-Correlation (AC), which is an industrial standard for ultrashort pulse diagnostic, is used for estimating the pulse duration. Unfortunately, intensity AC cannot be used to characterize the full electromagnetic field of the laser pulse. During the last 25 years a whole "zoo" of advanced techniques to characterize both the amplitude and phase of the field complex envelop were developed. The most popular among these methods

include Frequency-Resolved Optical Gating (FROG) [15], Spectral Phase Interferometry for Direct Electric-field Reconstruction (SPIDER) [16], and d-scan [17]. Still, there is always motivation to improve these techniques as there are pulses that are too complicated, too weak, or too short to be measured.

Here, we utilize sparsity-based information processing in diagnostics of ultrashort laser pulses. We develop and demonstrate, numerically and experimentally, the use of sparsity in three different applications. In Section 2, we demonstrate improvement of the resolution of a photodiode-oscilloscope system for measuring the intensity profiles of laser pulses when the profile can be represented compactly in a Gauss Hermite (GH) basis. As there is an infinite number of GH bases (Gaussian center and width are free parameters), our reconstruction algorithm uses only the measured signal to find the GH basis in which the sought pulse is the sparsest. In Section 3, we exploit sparsity for reconstructing profiles of pulses from intensity auto-correlator measurements. In this application, we explore pulses with Gaussian power spectra and low-order polynomial spectral chirp. We show that such pulses can be represented compactly using an over-complete set of GH functions. In Section 4, we apply sparsity-based information processing to improve XFROG: a technique for recovering the amplitude and phase of ultrashort laser pulses from cross-correlation frequency-resolved optical gating measurements.

2. Sparsity-based super-resolution in photodiode detection

High-speed photodiodes are widely used for direct measurements of pulse intensity profiles because of their simplicity, robustness, wide spectral bandwidth, small size, and low cost. The temporal resolution of high-speed photodiodes can get down to the picosecond (ps) regime. Intensity profile measurements at sub-ps resolution require more complex devices such as streak cameras and cross or autocorrelation techniques. The Radio Frequency (RF) spectral response function of photodiodes, acts as a low-pass filter (LPF), with a characteristic cutoff-frequency f_c (where $f_c \sim 1/T_c$, and T_c is the response time of the photodiode). If the laser pulse contains features at a time-scale that is close to (or shorter than) T_c then the output electronic signal deviates from the actual laser pulse waveform. In this case, de-convolution may extract the fast features in the pulse-shape by amplifying the RF high-frequency components of the output signal with the aim of "undoing" the LPF operation. However, the resolution of de-convolution is fundamentally limited by noise, which is present in all detectors, because a large factor amplifies small errors in the high-frequency spectral regions of the output signal. Consequently, deconvolution processes cannot recover information that is contained in spectral regions in which the signal to noise ratio is smaller than the LPF spectral response function (typically corresponding to the $f > f_c$ spectral region) [18].

Here we propose and demonstrate a scheme for reconstructing the temporal shape of laser pulses that can be represented compactly using a Gauss Hermite (GH) basis at a resolution that exceeds the resolution limit of deconvolution processes. In particular, we recover the information at frequencies way beyond the cutoff frequency, f_c. Our reconstruction algorithm uses only the direct output signal of the photodiode and the prior knowledge that the sought signal is sparse in one (unknown) member of the GH bases. The reconstruction scheme implements the Basis Pursuit (BP) algorithm, which is a well-known method for recovering sparse data from an under-determined linear system of equations [19]. Importantly, the BP algorithm is robust to noise in the measured data and thus is very attractive for short pulse measurements. Our reconstruction scheme relies on the fact that the laser pulse can be represented compactly in a GH basis. However, GH functions, given by $GH_n = H_n(t)\exp(-(t-t_0)^2/\Delta t)$ where H_n is a Hermite polynomial of order n, in fact, are an infinite family of bases, when the center position t_0 and the width of the Gaussian function Δt are free parameters. Our algorithm includes a stage for automatic determination of a GH basis from the measured signal only. Specifically, the center position t_0 is determined by the "center of mass" of the blurred pulse obtained by deconvolution. Then, to determine the width parameter Δt, we run

our algorithm for a set of admissible width values and choose the solution in which the reconstructed pulse is represented most compactly.

An experimental demonstration of our scheme is presented in Fig. 1(a). A "slow" photodiode detects a laser pulse with 1000 ps rise time and an oscilloscope samples the electronic signal. For comparison only, we also detect the same pulse with a "fast" photodiode (175 ps rise time). To characterize our measurement system, we first measure the impulse response function (IRF) (and calculate from it its spectral transfer function) of the photodiodes by detecting a 30-fs pulse [Figs. 1(b) and 1(c)].
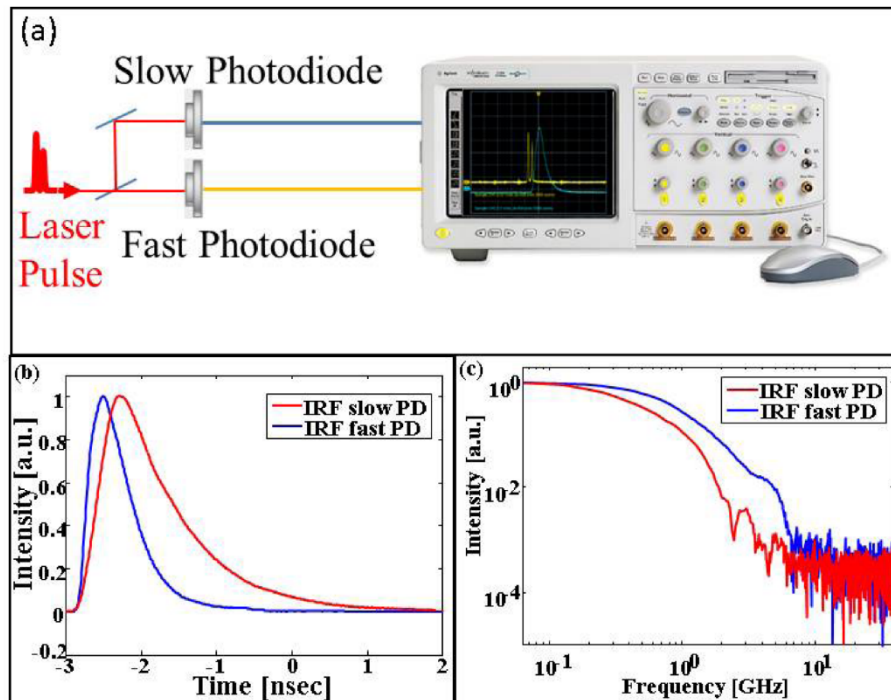

Fig. 1. Experimental setup: a laser pulse is probed by slow (1000 ps rise-time) and fast (175 ps rise-time) photodiodes and an oscilloscope with 6 GHz bandwidth. Impulse response functions (b) and corresponding spectra (c) of the slow (red) and fast (blue) photodiodes.

Next, to demonstrate our technique, we construct a structured laser pulse containing three peaks by splitting and recombining three delayed replicas of the laser pulse (FWHM = 150 ps). Figure 2(a) shows a measurement of the structured pulse by the slow and fast photodiodes, with their associated Fourier spectra shown in Fig. 2(b). Next, we apply Wiener deconvolution to the output signals from the "slow" and "fast" photodiodes (Fig. 2(c) red dashed and blue dashed curves respectively). The de-convolved pulse from the fast photodiode serves as a reference pulse for comparison purpose only. Clearly, the de-convolution approach completely fails to reconstruct the structures of the pulse when it is applied to the measured signal from the slow photodiode. Next, we apply our sparsity-based approach. We first determine the center of the GH functions according to the "center of mass" of the deconvolved pulse (Fig. 2(c) red dashed curve). Then, we run our sparsity-based reconstruction algorithm while scanning the width parameter: Δt, Fig. 2(d) shows the number of non-zero elements in each such reconstruction (elements that are larger than 0.01) as a function of Δt. Importantly, the similar scheme of 1D signal retrieval was implemented in [2], and it was shown to be robust to noise and applicable to signals constructed from unit-cell (Gaussians or rectangles) with variable width. The final reconstructed pulse, which corresponds to the pulse with a minimal number of elements ($\Delta t = 25$ps in Fig. 2(d)), is shown

in Fig. 2(e). For comparison, that plot also shows the reference pulse as well as the pulse obtained by applying our sparsity-based reconstruction algorithm using the measured signal by the fast photodiode. The sparsity-based reconstructed pulse-shape using the signal from the slow photodiode matches very well the measured pulse through Wiener de-convolution and sparsity-based using the signal from the fast photodiode. This correspondence shows that our sparsity-based reconstruction accomplishes super-resolution, significantly better than Wiener deconvolution. The power spectra of these pulses
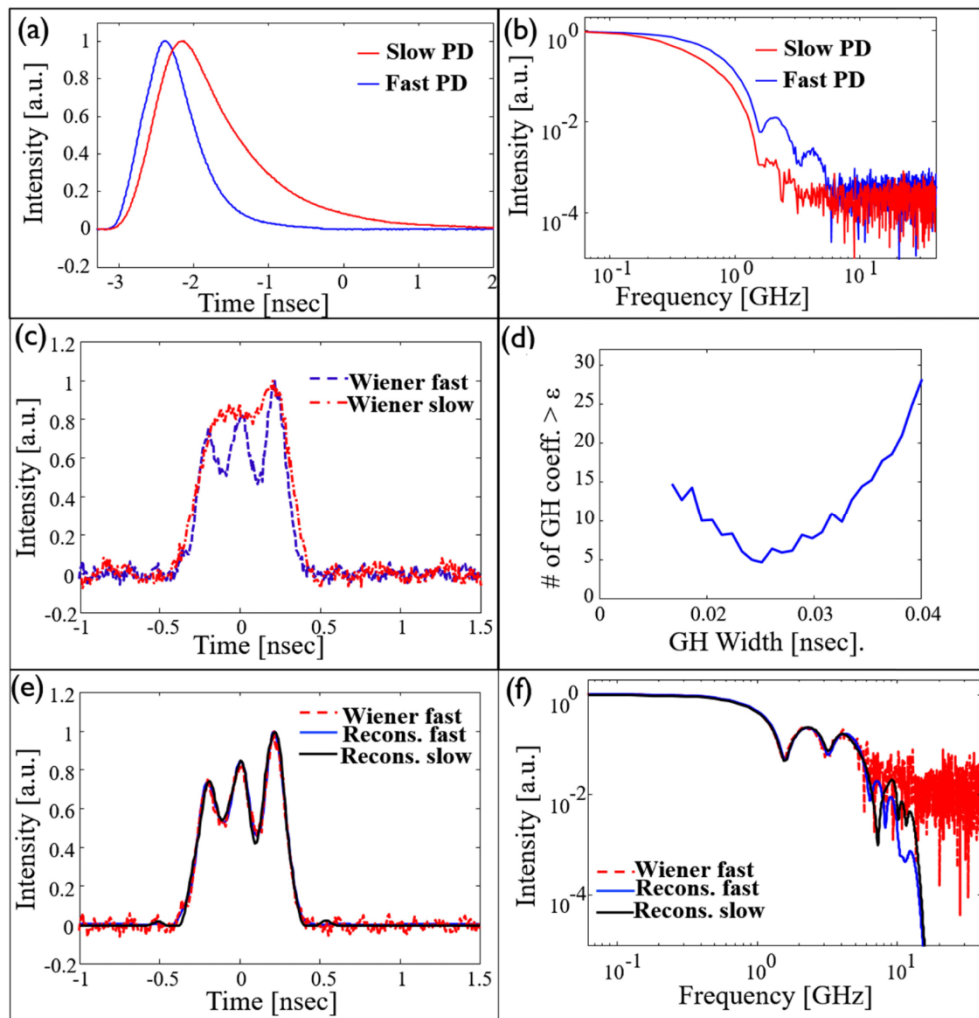

Fig. 2. Direct signals (a) and corresponding spectra (b) when the laser pulse is probed by the slow (red) and fast (blue) photodiodes. (c) Reconstructed pulse-shapes by implementing Wiener de-convolution. (d) The number of non-zero elements in each sparsity-based reconstruction (see text above). (e) The sparsity-based reconstructions with the slow (solid black) and the fast (solid blue) photodiodes as well as the Wiener de-convolution with a fast photodiode (dashed red) are all quite similar: the three-peak waveform is well captured, and their spectra (f) nicely match up to 5 GHz. On the other hand, without utilizing sparsity, the Wiener de-convolution with the slow photodiode ((c) (dash red) does not capture the peaks of the waveform and its associated spectrum starts to deviate from the other spectra at 1 GHz. In these experiments, the sparsity-based reconstruction with the slow photodiode exhibits super-resolution of up to 5 times relative to the Wiener de-convolution.

are shown in Fig. 2(f), indicating that the resolution of the sparsity-based reconstruction from the slow photodiode is ~5 times better than Wiener deconvolution.

In this section, we demonstrated that sparsity can significantly increase the resolution of photodiodes for pulse-shape measurements, by at least a factor of 5. Thus, our technique may be used for measuring sub-picoseconds pulses with current ultrafast photodiodes. Similarly, our approach can be implemented in various other types of pulse-measurement techniques, in which the measured pulse is correlated with a response function of the device (e.g., streak cameras).

3. Intensity waveform reconstruction from intensity autocorrelation

Intensity autocorrelators have been used for estimating the pulse duration of ultrashort laser pulses since the 1960s [20]. The AC trace of a pulse is given by $I_{AC}(\tau) = \int I(t)I(t-\tau)dt$ where $I(t)$ is the intensity profile (waveform) of the pulse. The AC signal is obtained by nonlinear interaction (typically second harmonic generation (SHG) or two-photon absorption) between the laser pulse and its replica with a tunable delay, τ. While advanced methods for characterization of ultrashort laser pulses were developed in the mid-1990s [21], intensity AC is still often used because the measurement is relatively simple, fast and efficient. However, pulses with significantly different intensity profiles can produce indistinguishable AC traces, i.e. intensity AC has non-trivial ambiguities [22]. Adding the measurement of the power spectrum helps but does not entirely remove the ambiguity [22]. Using the positivity of the intensity profile and the support (localization) as prior information also do not remove the ambiguity in this problem [17]. Here, we utilize a sparsity prior together with the positivity of the intensity for reconstructing the intensity profiles of pulses from their intensity autocorrelations. Specifically, we assume that the intensity waveforms of the pulses are sparse in a set of GH functions. We also show that this assumption is valid for pulses with Gaussian power spectra and low-order polynomial chirps, which is often the case with many ultrafast laser pulses [23].

Reconstruction of intensity profiles from their autocorrelation function is equivalent to a 1D phase retrieval problem, as the Fourier transform of the autocorrelation corresponds to $|\hat{I}(\omega)|^2$ where $\hat{I}(\omega)$ is the Fourier transform of the intensity profile. Thus, one needs to retrieve the spectral phase of $\hat{I}(\omega)$ to decipher $I(t)$ from its autocorrelation measurement. In this application, we use the sparsity-based phase retrieval algorithm termed GESPAR (GrEedy Sparse PhAse Retrieval) for reconstructing intensity profiles from their AC measurements [24], the same algorithm that we used for reconstructing 1D images from their diffraction intensities [3]. In addition to sparsity, we use positivity of intensity as a constraint. Accordingly, we slightly modify the original GESPAR algorithm by replacing the damped Gauss-Newton step by a more general step involving minimization of constrained nonlinear multivariable function [25]. In practice, this step is performed by using the MATLAB Optimization Toolbox and Constrained Nonlinear Optimization function (fmincon) with an interior-point algorithm.

First, we show that the intensity profiles of ultrashort laser pulses with Gaussian power spectra and low-order polynomial spectral chirp can be represented compactly using an over-complete set of GH functions. In this work, we use the frame, $\Psi_{n,m,q} = H_n(t)\exp(-(t- t_m)^2/\Delta t_q)$ where H_n ($n = 0,1,2,3...N$) is the nth-order Hermite polynomial, Δt_q ($q = 1,2...Q$) are width parameters and t_m (with $m = 1,2,3...M$) are center parameters. We choose $N = 17$, $M = 10$ and $Q = 1$, which means that the frame consists of only 180 functions. We construct the appropriate frame for each pulse separately using only its measured (or calculated) AC trace. For each AC trace, we use a width parameter that corresponds to 0.7 times the FWHM of the AC trace while the center parameters are distributed uniformly on the interval of the sampled (or calculated) AC.

We now examine the range for which GESPAR with the above frame of GH functions gives reliable reconstructions. We start by randomly forming 100 intensity profiles, and their autocorrelations, for each sparsity level, s (the sparsity level of an intensity profile corresponds to the minimal number of GH functions from the frame that are required for its representation). Then, we use our phase-retrieval algorithm on the autocorrelations with added noise (45dB SNR). We consider the recovery to be successful if the Normalized Mean Square Error (NMSE) between the original and recovered pulses is smaller than 0.02. For example, the original and reconstructed electric field profiles of a pulse with $s = 16$ are shown in Fig. 3(a). The calculated probability for successful recovery is shown in Fig. 3(b). It indicates that the probability for successful reconstruction of pulses with $s \leq 17$ is very high (practically equal to one) and it then drops fast with increasing sparsity. Figure 4 demonstrates the successful reconstruction of electric field profiles from their ACs under the assumption that the electric field profiles are sparse in a frame of GH functions. However, it is important to study whether this assumption is general, characterizing most ultrafast laser pulses generated in experiments. To address this important issue, we show that indeed ultrashort laser pulses with low-order polynomial spectral phase and corresponding ACs with limited support tend to be sparse in our frame of GH functions. Furthermore, we demonstrate that there is a range of parameters in which our method reconstructs the electric field profile with practically 100% probability and reliability. We present this feature through an example.
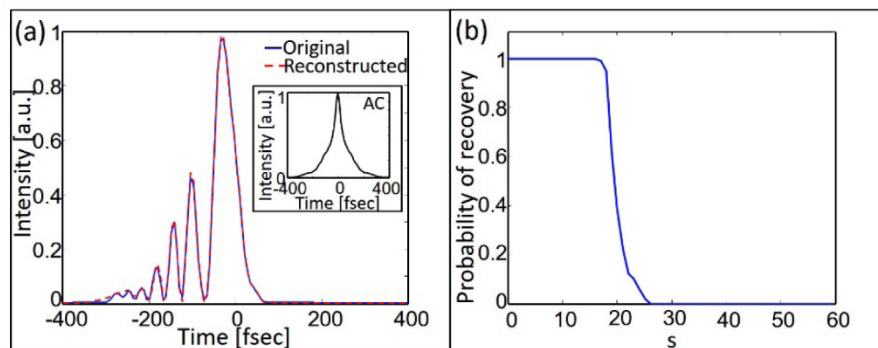

Fig. 3. Calculated sparsity-based reconstruction of electric field profiles from their autocorrelations using GESPAR under the assumption that the pulse is sparse in the GH frame. (a) Original (blue solid) and reconstructed (dashed red curve) electric field profiles. The original electric field profile is comprised of 16 GH functions. The inset shows the autocorrelation signal of the original pulse. (b) Reliable recovery probability using the sparsity-based method versus sparsity level, i.e. the minimum number of GH functions that can represent the electric field profile of the pulse. The recovery is certain (~100%) for $s \leq 17$.

We start by numerically producing sets of laser pulses with a Gaussian power spectrum, as displayed in Fig. 4(a). Each set is characterized by a support range of the autocorrelation function of the pulses: SAC ± 0.02SAC, where we define the support length, SAC, as the longest distance between delays for which the AC function is 0.001 of the AC peak. Of course, the AC support is directly related to the pulse duration. For comparison, the AC support and the FWHM pulse duration of the transform limited pulse (which has flat phase) are 93 fs and 34 fs, respectively. Each set of pulses consists of 5000 pulses with 5th-order polynomial spectral chirps with randomly produced coefficients. An example of a pulse with AC support length of 700 fs and the specific spectral chirp plotted in Fig. 4(a) is shown in Fig. 4(b). Next, we calculate the most compact representation in our frame for each pulse in every set, by solving an L1 minimization problem with up to 1% NMSE [19]. Figure 4(c) shows the distributions of pulses in three sets (AC support lengths 400, 600 and 800 fs) as a function of their sparsity level. Clearly, almost all the pulses are sparse in our frame of 180 GH functions. Recall that according to Fig. 3(b), our algorithm reconstructs pulses with $s \leq 17$

at 100% certainty. We therefore calculate and plot in Fig. 4(d), the fraction of pulses in each set with s≤17. As shown there, there is a significant range (AC support length ≤ 500 fs) for which accurate reconstruction is granted. The probability for correct reconstruction then decreases with increasing AC support. To summarize this section, Figs. 3 and 4 presented reliable sparsity-based pulse recovery. In Fig. 3, we do not assume a given (known) sparsity basis for all relevant pulses, instead, we calculate the range of appropriate GH functions by spanning the t_m parameter from limits defined by the measured data. In doing that, we accomplish sparsity-based phase-retrieval of 1D information, without prior knowledge of the exact basis in which the information is sparse. Then, in Fig. 4 we show that sparsity in this flexible GH frame is related to prior knowledge that the measured pulse has a low-order polynomial chirp. We envision implementing our reconstruction method whenever it is known in advance that the spectral phase of the pulse is polynomial. If the power spectrum of the pulse is measured, then one can use the procedure presented in Fig. 4 for calculating the probability that the reconstruction is correct. Finally, we note that the probability for correct reconstruction should improve by increasing the number of functions in the frame (i.e. by increasing N, M, or Q).
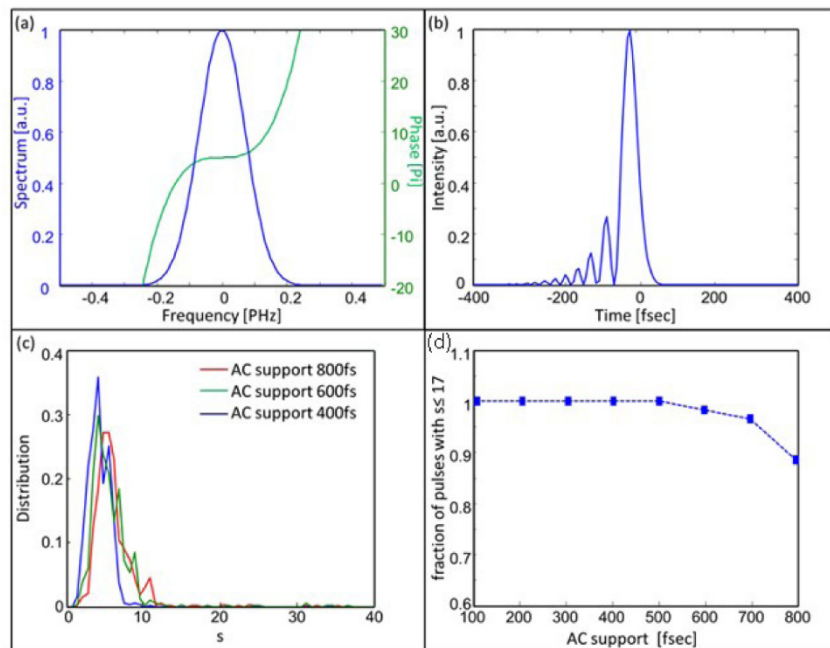

Fig. 4. A demonstration that pulses with low-order polynomial spectral chirps can be represented compactly in our GH frame. (a) Gaussian power spectrum used in the current simulation (blue curve) and a specific example of a 5th-order polynomial spectral phase (green curve). (b) Waveform (pulse intensity profile in time) that corresponds to the spectrum and spectral phase in (a). (c) Sparsity level of pulses - all with the same power spectrum shown in (a), and all with 5th-order polynomial spectral chirps, as a function of sparsity, for three AC support lengths (see text). (d) The fraction of pulses with s≤17 as a function of AC support length. As shown here, correct reconstruction of all pulses with AC support length ≤ 500 fs has almost 100% certainty.

Next, we demonstrate the experimental implementation of our sparsity-based 1D phase retrieval for reconstruction of the intensity profile of a pulse from its AC measurement. We construct a pulse with a structured intensity profile by passing, through a 10mm thick sample of fused silica, an approximately transform-limited ultrashort laser pulse with a pulse duration of ~30 fs. Generally, the spectral chirp of a pulse generated in this way should be well

approximated by a 5th-order polynomial expression. We measure the AC of this pulse (Fig. 5(a)) using an SHG autocorrelator. For reference, we also measure the pulse using an SHG FROG system [15]. The measured and reconstructed spectrograms (FROG traces) are shown in Figs. 5(b) and 5(c), respectively. Figure 5(d) shows the pulse (in the frequency domain) reconstructed by the standard (singular value decomposition) FROG recovery algorithm. The reconstruction is very good (the NMSE between the measured and reconstructed spectrograms is $8.3 \times 10\text{-}6$). The reconstructed intensity profiles using the sparsity-based algorithm from the measured intensity AC trace and the FROG method are depicted in Fig. 5(e), clearly demonstrating that the sparsity-based reconstruction is very good (the NMSE between the intensity profiles is 2%). Figure 5(f) shows the representations of the two reconstructions in the frame of GH functions. As seen in Fig. 5(f), the discrepancy between the two recovery methods results from several GH functions with coefficients that are smaller than the threshold parameter in GESPAR, which corresponds to the noise level in the measurement ~38 SNR. That is, decreasing the noise in our experimental system should lead to increased accuracy of the reconstruction.

Finally, it is worth noting how one can gain confidence in the sparsity-based reconstruction from the AC measurement, without assuming in advance that the pulse is sparse in the set of GH functions. For example, assuming that the power spectrum of the pulse (shown in Fig. 5(d)) is measured, we apply the procedure described in Fig. 4 and calculate the distribution of pulses with 5th-order polynomial chirps and AC support length of 600 fs (as derived from the measured AC trace) as a function of sparsity level. The distribution is displayed in Fig. 5(g), shows that almost all of the possible pulses are indeed sparse. For example, the sparsity level of 96.4% of the pulses is $s \leq 17$. Notably, if the power spectrum of the pulse is Gaussian, then by recalling that our algorithm reconstructs such pulses with $s \leq 17$ at practically 100% certainty (Fig. 3(b)), we could assign a >96.4% reconstruction certainty.
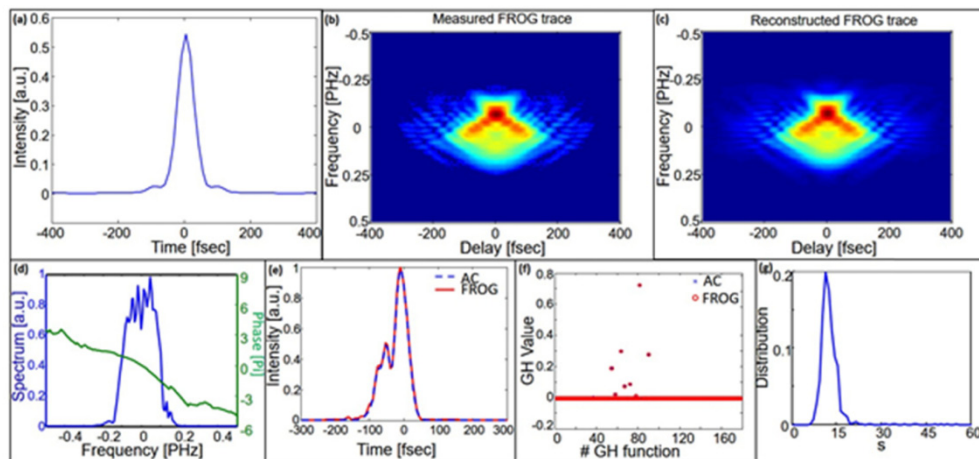

Fig. 5. Experimental demonstration of reconstructing the laser intensity profile from its autocorrelation trace. For comparison, we also characterize the pulse using SHG FROG. (a) Measured intensity autocorrelation trace. (b) Measured SHG FROG interferogram. (c) Reconstructed interferogram (NMSE is 8.3x10-6). (d) Reconstructed pulse (blue curve) and spectral phase (green curve) - using the standard (singular value decomposition) FROG recovery algorithm. (e) The reconstructed intensity profiles using the sparsity-based algorithm from the measured intensity AC trace (blue dashed line) and the FROG method (solid red line), clearly showing that the sparsity-based reconstruction is very good (the NMSE between the intensity profiles is 2%). (f) The population of the reconstructed pulses in the GH basis (g) The distribution of pulses with power spectrum in plot (d), 5th-order polynomial spectral phase and intensity autocorrelation support length of 600 fs as a function of sparsity-level.

4. Sparsity in XFROG

Cross-correlation frequency-resolved optical gating (XFROG) is used for measuring the amplitude and phase of ultrashort laser pulses [26]. This technique is especially effective for measuring weak pulses, because it relies on sampling the unknown pulse with a much stronger known pulse through a sum frequency generation process, overall having reasonable SNR. Other techniques, such as FROG [27, 28], SPIDER [16], and d-scan [17] (an increasingly popular method for all-inline pulse retrieval), measure signals that are square-proportional to the power of the unknown pulse, thus obtaining low SNR at acquisition. In XFROG, the reconstruction algorithm retrieves the pulse (amplitude and phase) from a measured spectrogram, i.e., a two-dimensional intensity map, which is obtained by frequency resolving the nonlinear intensity cross-correlation between the measured pulse and a known reference pulse. The current retrieval algorithm is based on the generalized projections method [29], thus requiring to measure all non-zero frequency components of the spectrogram. This condition sets an upper limit on the length of the nonlinear crystal due to the phase matching window.

Here, we propose and demonstrate an XFROG trace inversion algorithm that utilizes the compact representation of an ultrashort (femtosecond) laser pulse. First, we show that ultrashort pulses can often be represented compactly in the Von-Neumann (VN) basis [30–32]. Then, we modify the GESPAR algorithm [24] to utilize the sparse representation of pulses in the VN basis in an XFROG reconstruction. We demonstrate the robustness to noise and super-resolution (i.e. reconstruction from spectrally filtered XFROG spectrograms) of this reconstruction algorithm. Finally, we demonstrate the technique in experiments.

The method is based on the utilization of prior information, in the VN basis [30], a feature that was used for optimizing pulse shaping [31], 2D electronic spectroscopy [33] and pulse characterization using angular streaking [34]. The VN basis [35] represents a discrete complex signal in a 2D complex joint time-frequency (JTF) domain. The main advantage of this basis is the localization of the base functions in the JTF domain. This is a direct result of the time and frequency Gaussian intensities of the base functions, that are centered around a single point in the JTF space, i.e. (ω_n, t_m).

In the frequency domain, VN base functions are given by:

$$\tilde{\alpha}_{\omega_n,t_m}(\omega) = \left(\frac{2\alpha}{\pi}\right)^{\frac{1}{4}} \exp\left\{-\alpha(\omega-\omega_n)^2 - it_m(\omega-\omega_n)\right\} \tag{1}$$

where $\alpha = T/2\Omega$, T and Ω, are the total time and frequency spans. The Fourier transform of each such base function is a Gaussian in the time domain, centered around t_m. Here, we choose the centers of these Gaussians (ω_n, t_m) to be equally spaced points in the JTF domain, such that $(n,m) \in [1,\sqrt{N}]$, hence $\omega_n = n\Omega/\sqrt{N}$, $t_m = nT/\sqrt{N}$ where N is the number of sampled points of the pulse. To demonstrate that ultrashort pulses can indeed most often be represented compactly in the VN basis, we calculate the sparsity level of three sets of pulses in the VN representation and time basis. We create these sets of pulses by adding random spectral phase to a Gaussian spectral amplitude $S(f) \propto \exp(-(f-f_c)^2/2\sigma_f^2)$ with bandwidth $\sigma_f = 80$ THz and central frequency $f_c = 751$ THz, when the total number of samples N is 256, over a spectral range $\Omega = 800$ THz. Then, we sort the pulses into three groups according to their pulse duration (or time-bandwidth product, TBP): 40-70 fs (3.2-5.6), 70-150 fs (5.6-12), and 150-300 fs (12-24). We define the pulse duration by the full width at 10% of the pulse peak. We also define the sparsity level S_{basis} of a specific pulse in a certain basis as the minimal number of coefficients needed to represent a pulse with less than 0.01 variation from the original one in the time domain. In this definition of sparsity, the variation is required because we deal with general pulses that were not specifically constructed from several VN basis functions. The variation is calculated by the L2 distance between the original and the sparsely

represented pulses. The sparsity of our pulses in the frequency basis is equal to 142 coefficients on a grid of $N = 256$ (easily calculated by removing the smallest samples in the frequency domain until 0.01 of the total power is lost), which is generally not considered sparse. Figure 6(a) displays the cumulative histogram for the sparsity in time S_t and in the VN base is S_{VN} for the three different sets. Clearly, the pulses can be represented more compactly when the VN basis is used.

The efficiency of using the VN basis is more significant for pulses with larger TBP, up to a limit, when the number of VN coefficients exceeds the minimum number of coefficients needed in the frequency domain. Figures 6(b)-6(j) show three specific examples, one from each set. The time-varying intensity and phases of the pulses are shown in the left column.
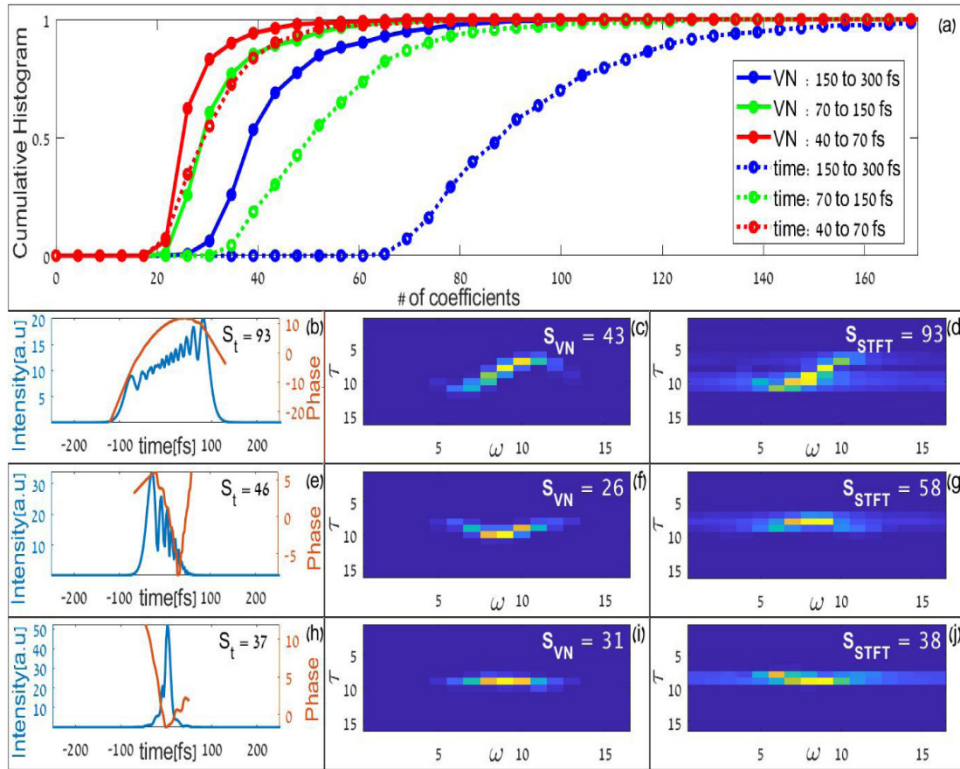

Fig. 6. Compactness of ultrashort laser pulses in the Von-Neumann (VN) representation. (a) Normalized cumulative histogram for obtaining good representations of pulses as a function of the minimal number of non-zero coefficients using VN basis (solid lines) and time basis (dash lines) for sets of pulses with pulse duration in the range 150-300 fs (blue lines), 70-150 fs (green lines) and 40-70 fs (red lines). (b-j) examples of three pulses with significantly different pulse durations showing: (b,e,h) time-varying intensities (blue line) and phases (red line), (c,f,i) VN representations in the VN basis and (d,g,j) representations in the STFT basis. S_t, S_{VN} and S_{STFT} correspond to the sparsity levels in the time, VN and STFT bases.

The central column displays the VN representation of the pulses while, for comparison, their representation in the short time Fourier transform (STFT) - a popular JTF basis [36] - is shown in the right column. The sparsity levels S_t, S_{VN} and the sparsity level of the STFT transform S_{STFT} are denoted in Figs. 6(b)-6(j) (The STFT is less compact than the VN and time representations, thus we do not add the STFT method to the comparison in Fig. 6(a)).

Next, to reconstruct the pulse from its XFROG trace, we adapt the GESPAR algorithm and explore the complex nature of the VN coefficients. Specifically, GESPAR obtains a vector of the XFROG trace measurements $y \in \mathbb{R}^{N_t \cdot N_\omega}$ (N_t, N_ω are the number of samples in

time and spectrum, respectively), while the reconstructed signal, P_t, and its representation coefficients in the VN basis, v, are complex: $P_t \in \mathbb{C}^N$ and $v \in \mathbb{C}^N$. We denote by $F^r \in \mathbb{C}^{N_t \cdot N_\omega \times N}$ the matrix that satisfies $F^r = LD$, where $L \in \mathbb{C}^{N_t \cdot N_\omega \times N}$ is the XFROG operator matrix and $D \in \mathbb{C}^{N \times N}$ denotes the transform operator from the frequency domain to the VN basis. We use the bi-orthogonal form of VN, therefore D is the pseudo-inverse of the VN basis matrix A, whose columns are base vectors $\tilde{\alpha}_{\omega_n,t_m}(\omega)$ (see ref [37] for more details). We also require the sparsity level of v to be smaller than some value s. Using the notation above, the GESPAR minimization problem becomes.

$$\hat{v} = \arg\min_v \left\{ \sum_{i=1}^{N^2} \left(\left| F_i^r v \right|^2 - y_i \right)^2 \right\}$$

$$s.t. |v|_0 \le s, supp(v) \subseteq \{1,2,...,n\}. \qquad (2)$$

To deal with the fact that the VN coefficients are complex, we modify GESPAR by using complex differentiation tools [38]. After this adjustment, we apply the GESPAR algorithm to recover complex field vectors from XFROG measurements.

We first investigate our sparsity-based reconstruction algorithm using numerical data. We specifically explore super-resolution, i.e. the recovery of pulses from partial XFROG traces. One can define a complete XFROG trace as $N \times N$ measurements for which the delay step
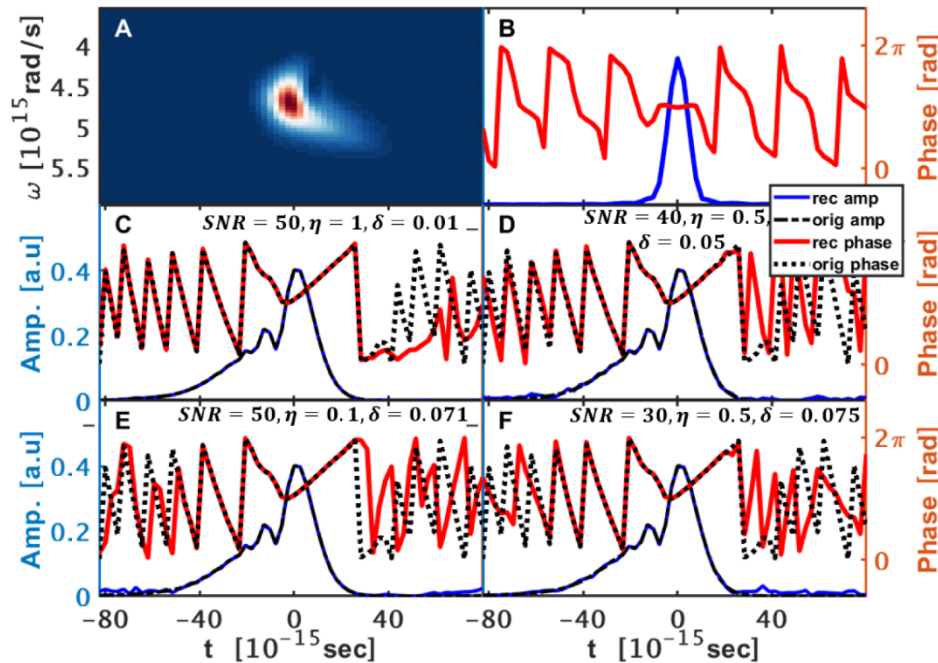

Fig. 7. Numerical demonstration of sparsity-based XFROG reconstruction when 20 coefficients describe the unknown pulse in VN basis, $S_{VN} = 20$. (A) XFROG trace (B) the gate pulse, amplitude (blue) and phase (red). (c)-(f) reconstructions of the unknown pulse, amplitude (blue) and phase (red), under different values of SNR and incompleteness, compared to the original pulse, amplitude and phase (black curves). The SNR, incompleteness parameter η, and reconstruction error, δ_1, are denoted in each plot.

and spectral resolution product should be $1/N$. Also, the bandwidth of the XFROG trace should be ~1.4 times larger than the bandwidth of the pulse power spectrum autocorrelation [39]. In this context, we define the incompleteness parameter [40] by

$$\eta = \frac{\# \text{ of pixels in the incomplete trace}}{\# \text{ of pixels in the complete trace}}$$

We specifically remove high-frequency data points, imitating the action of a low pass filter. Examples of reconstructions of pulses with $S_{VN} = 20$ and $S_{VN} = 25$ with different conditions of SNR and η are shown in Figs. 7 and 8, respectively.
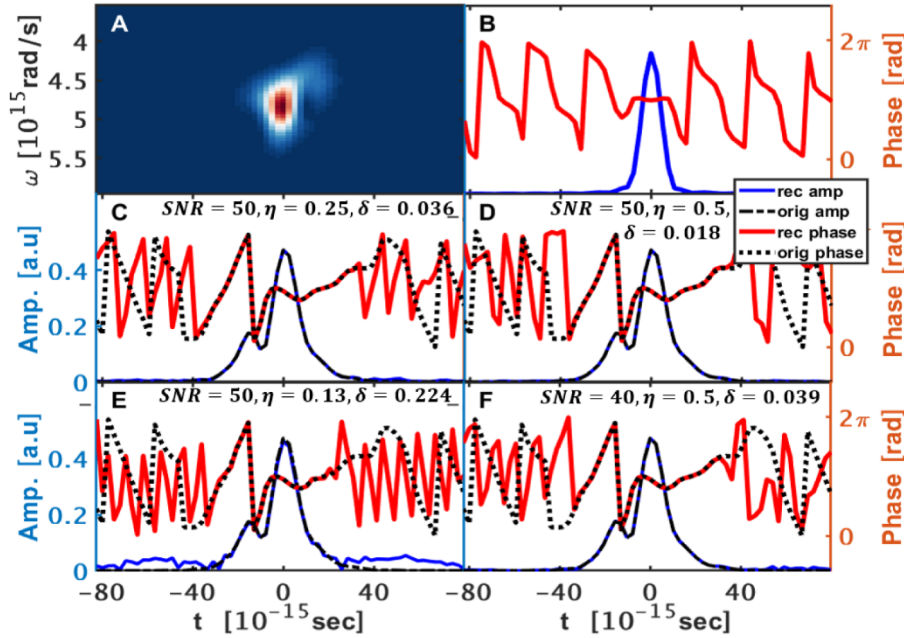

Fig. 8. Numerical demonstration of sparsity-based XFROG reconstruction when 25 coefficients describe the unknown pulse in VN basis, $S_{VN} = 25$. (a) XFROG trace (b) the gate pulse, amplitude (blue) and phase (red). (c)-(f) reconstructions of the unknown pulse, amplitude (blue) and phase (red), under different values of SNR and incompleteness, compared to the original pulse, amplitude, and phase (black curves). The SNR, incompleteness parameter, η, and reconstruction error, δ_1, are denoted in each plot.

Next, to test the performance of our algorithm at different SNR and η values, we construct 500 different pulses and their XFROG traces (with a fixed gate pulse) for three different sparsity levels $S_{VN} = 20$, 25 and 30. This is shown in Fig. 9. The pulses have a Gaussian spectrum with bandwidth $\sigma_f = 80$ THz and central frequency $f_c = 751$ THz, with a total number of samples $N = 64$ over a spectral range $\Omega = 800$ THz. We use a gate pulse $G(t)$, with the same spectrum and a time duration of $FWHM = 10fs$, to create XFROG traces. Then, we add White Gaussian Noise (WGN) to the XFROG traces to obtain simulated data at different SNR values. Finally, we reconstruct the pulses from their noisy and incomplete XFROG traces using our modified GESPAR algorithm relying on the VN basis. Figure 7 shows the reconstruction error $\delta_2(P,\dot{P}) = \text{arccps}(|<\dot{P}|P>|/(\sqrt{<\dot{P}|\dot{P}>}\sqrt{<P|P>}))$ [41], as a function of the incompleteness parameter for the three different sparsity values and three different SNR levels. It shows that for small sparsity values, the reconstruction error can be quite low, even at low SNR and low η. For example, at $S_{VN} = 20$ and $SNR = 50$, $S_{VN} = 20$ and $SNR = 40$, as well as $S_{VN} = 25$ and $SNR = 50$ all yield reconstructions with ~0.1 error.

Finally, we demonstrate sparsity-based XFROG reconstruction in an experiment. We use pulses from a Ti:Sapphire laser and our home-made SHG FROG/XFROG system. We split a pulse using a beam-splitter (BS), and use one pulse for the gate pulse G(t) and the other one, which is passed through a glass of 1cm thickness, as the unknown pulse P(t). For reference,

we measure each of these pulses independently using FROG. The measured gate pulse is shown in Fig. 10(a). The measured complete XFROG trace is shown in the inset of Fig. 10(b) which consists of 14 fs sampling delay with 64 samples in time and 64 samples of the spectrum, conserving the Fourier relation $\Delta\omega\cdot\Delta t = 1/N$. Figure 10(b) shows the spectrally filtered XFROG trace after 48 spectral lines were zeroed, yielding an $\eta = 0.25$ trace, that we use for reconstruction. Figure 10(c) shows the XFROG trace recovered that was reconstructed by using the measured and filtered XFROG trace (Fig. 10(a)). Clearly, the sparsity-based algorithm retrieves the non-sampled parts of the XFROG trace (the discrepancy between the recovered and measured traces is $\delta_1 = 0.19$). The FROG and filtered XFROG reconstructions of the unknown pulse are shown in Fig. 10(d), showing good correspondence.
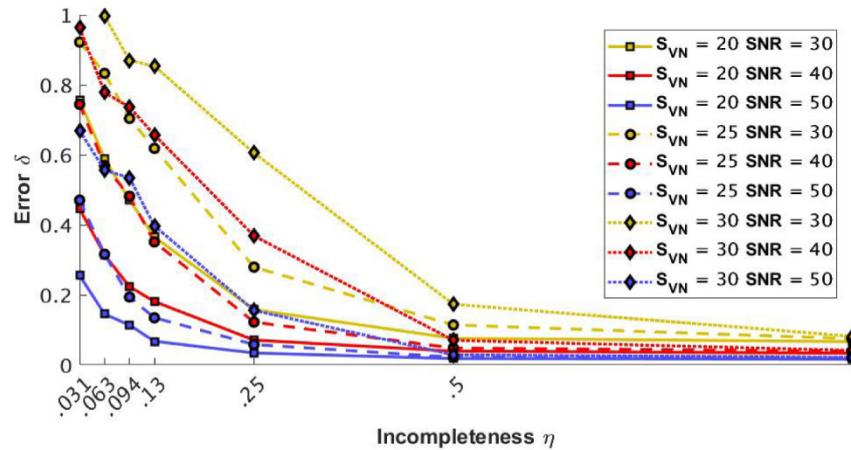

Fig. 9. Numerical investigation of sparsity-based XFROG reconstruction versus incompleteness, η, SNR values 30, 40 and 50 and VN sparsity levels 20, 25, and 30.
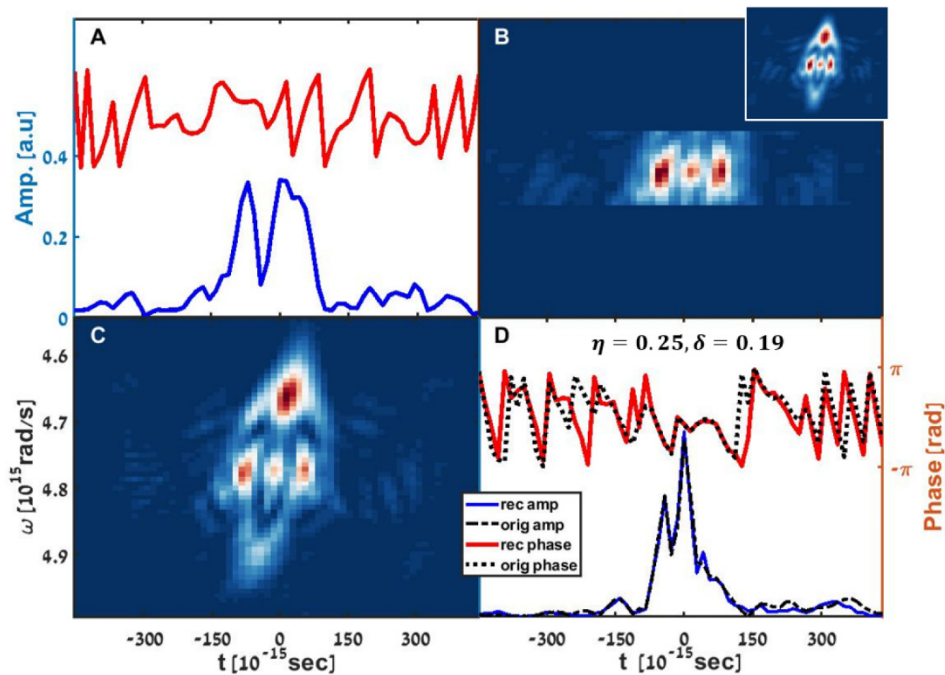

Fig. 10. Experimental demonstration of sparsity-based XFROG reconstruction using an incomplete XFROG trace. (a) amplitude (blue) and phase (red) of the gate pulse. (b) Measured

XFROG trace with η = 0.25, (i.e., 16 frequencies out of 64 in the complete XFROG trace shown in the inset). (c) Recovered XFROG trace using the spectrally filtered XFROG trace and the sparsity-based reconstruction algorithm. (d) The recovered unknown pulse (amplitude in blue and phase in red) on top of the amplitude and phase curves measured through FROG. The error between the reconstructions is 0.19.

5. Conclusions

We introduced the concept of using sparsity as prior information in the characterization and shape recovery of ultrashort laser pulses and specifically applied it in three very different techniques: enhancing the resolution of photodiodes, recovering intensity profiles from intensity auto-correlation measurements and XFROG reconstruction from incomplete spectrograms. Although neural network techniques exist and can automatically extract suitable bases from the data, they require more than tens of thousands of measurements and their pulse reconstructions [42], which is practically unreasonable. Hence, we believe that obtaining and exploiting the sparsity prior will be useful in many more methods for diagnostics of ultrashort laser pulses. We anticipate that this would allow decreasing the minimum number of spectral lines required for complete reconstruction of pulses from their FROG traces [40,43]. Likewise, using the sparsity prior increases the maximum number of recovered pulses in multiplexed FROG [44], and generally leads to improved algorithmic recovery of pulses from indirect measurements at low SNR values. We believe that future works will find more examples of sparsifying bases/frames that will open new possibilities for improved diagnostic methods for a variety of different applications.

References

1. M. F. Duarte, M. A. Davenport, D. Takhar, J. N. Laska, T. Sun, K. F. Kelly, and R. G. Baraniuk, "Single-pixel imaging via compressive sampling," IEEE Signal Process. Mag. **25**(2), 83–91 (2008).
2. A. Szameit, Y. Shechtman, E. Osherovich, E. Bullkich, P. Sidorenko, H. Dana, S. Steiner, E. B. Kley, S. Gazit, T. Cohen-Hyams, S. Shoham, M. Zibulevsky, I. Yavneh, Y. C. Eldar, O. Cohen, and M. Segev, "Sparsity-based single-shot subwavelength coherent diffractive imaging," Nat. Mater. **11**(5), 455–459 (2012).
3. P. Sidorenko, O. Kfir, Y. Shechtman, A. Fleischer, Y. C. Eldar, M. Segev, and O. Cohen, "Sparsity-based super-resolved coherent diffraction imaging of one-dimensional objects," Nat. Commun. **6**(1), 8209 (2015).
4. S. Gazit, A. Szameit, Y. C. Eldar, and M. Segev, "Super-resolution and reconstruction of sparse sub-wavelength images," Opt. Express **17**(26), 23920–23946 (2009).
5. Y. Rivenson, A. Stern, and B. Javidi, "Compressive Fresnel Holography," J. Disp. Technol. **6**(10), 506–509 (2010).
6. O. Katz, Y. Bromberg, and Y. Silberberg, "Compressive ghost imaging," Appl. Phys. Lett. **95**(13), 131110 (2009).
7. L. Tian, J. Lee, S. B. Oh, and G. Barbastathis, "Experimental compressive phase space tomography," Opt. Express **20**(8), 8296–8308 (2012).
8. J. Oliver, W. Lee, S. Park, and H.-N. Lee, "Improving resolution of miniature spectrometers by exploiting sparse nature of signals," Opt. Express **20**(3), 2613–2625 (2012).
9. M. Mutzafi, Y. Shechtman, Y. C. Eldar, O. Cohen, and M. Segev, "Sparsity-based Ankylography for Recovering 3D molecular structures from single-shot 2D scattered light intensity," Nat. Commun. **6**(1), 7950 (2015).
10. Y. C. Eldar and G. Kutyniok, *Compressed Sensing: Theory and Applications*, 1st ed. (Cambridge University, 2012).
11. S. Gleichman and Y. C. Eldar, "Blind compressed sensing," IEEE Trans. Inf. Theory (2011).
12. J. M. Duarte-Carvajalino and G. Sapiro, "Learning to sense sparse signals: simultaneous sensing matrix and sparsifying dictionary optimization," IEEE Trans. Image Process. **18**(7), 1395–1408 (2009).
13. T. Nagatsuma, M. Yaita, M. Shinagawa, K. Kato, A. Kozen, K. Iwasuki, and K. Suzuki, "Electro-optic characterization of ultrafast photodetectors using adiabatically compressed soliton pulses," Electronics Letters. **30**(10), 814–816 (1994).
14. P.A. Janamagi, "Breaking the 100-fs barrier with a streak camera," Proc. SPIE 5194, Fourth-Generation X-Ray Sources and Ultrafast X-Ray Detectors. 171–183 (2004).
15. R. Trebino, K. W. DeLong, D. N. Fittinghoff, J. N. Sweetser, M. A. Krumbügel, B. A. Richman, and D. J. Kane, "Measuring ultrashort laser pulses in the time-frequency domain using frequency-resolved optical gating," Rev. Sci. Instrum. **68**(9), 3277–3295 (1997).
16. C. Iaconis and I. A. Walmsley, "Spectral phase interferometry for direct electric-field reconstruction of ultrashort optical pulses," Opt. Lett. **23**(10), 792–794 (1998).

17. M. Miranda, C. L. Arnold, T. Fordell, F. Silva, B. Alonso, R. Weigand, A. L'Huillier, and H. Crespo, "Characterization of broadband few-cycle laser pulses with the d-scan technique," Opt. Express **20**(17), 18732–18743 (2012).
18. S. M. Riad, "The deconvolution problem: An overview," Proc. IEEE **74**(1), 82–85 (1986).
19. S. S. Chen, D. L. Donoho, and M. A. Saunders, "Atomic decomposition by basis pursuit," SIAM J. Sci. Comput. **20**(1), 33–61 (2001).
20. J. A. Armstrong, "Measurement of picosecond laser pulse widths," Appl. Phys. Lett. **10**(1), 16–18 (1967).
21. I. A. Walmsley and C. Dorrer, "Characterization of ultrashort electromagnetic pulses," Adv. Opt. Photonics **1**(2), 308 (2009).
22. J.-H. Chung and A. M. Weiner, "Ambiguity of ultrashort pulse shapes retrieved from the intensity autocorrelation and the power spectrum," IEEE J. Sel. Top. Quantum Electron. **7**(4), 656–666 (2001).
23. V. Bagnoud and F. Salin, "Global optimization of pulse compression in chirped pulse amplification," IEEE J. Sel. Top. Quantum Electron. **4**(2), 445–448 (1998).
24. Y. Shechtman, A. Beck, and Y. C. Eldar, "GESPAR: efficient phase retrieval of sparse signals," IEEE Trans. Signal Process. **62**(4), 928–938 (2014).